Journal of Inflammation Research

Dovepress
Taylor & Francis Group

Open Access Full Text Article

ORIGINAL RESEARCH

Yin-Hua Li-Shi Decoction Alleviated Atopic Dermatitis Through Regulating Th Cells Balance and Restoring Epithelial Barrier

Junchao Wu[1,2,*], Zongguang Tai[1,2,*], Congcong Zhu[1,2], Lisha Li[1,2], Jun Liu[1,2], Tianyou Ma[1,2], Bei Yin[1,2], Hanxue Zhou[1,2], Quangang Zhu[1,2], Zhongjian Chen[1,2]

[1]Shanghai Skin Disease Hospital, School of Medicine, Tongji University, Shanghai, 200443, People's Republic of China; [2]Shanghai Engineering Research Center for Topical Chinese Medicine, Shanghai, 200443, People's Republic of China

*These authors contributed equally to this work

Correspondence: Zhongjian Chen; Quangang Zhu, Shanghai Skin Disease Hospital, School of Medicine, Tongji University, 1278 Baode Road, Shanghai, 200443, People's Republic of China, Email aajian818@163.com; qgzhu@126.com

Purpose: Yin-hua Li-shi Decoction (YLD), a traditional Chinese medicine formulation, has been employed as a complementary therapy for atopic dermatitis (AD). Nevertheless, its precise therapeutic mechanisms remained unexplored.

Methods: YLD components were identified by LC-MS, and quality control was performed using HPLC. In vitro, flow cytometry was used to assess YLD toxicity and its effect on inhibiting pro-inflammatory macrophages. In vivo, AD mice model was induced by daily topical MC903 application on mice ears for 15 days. Mice received oral YLD (1.50, 3.00, or 6.00 g/mL) once daily for 14 days. Disease progression was tracked by measuring skin thickness in mice. ELISA, western blot, and immunohistochemistry were used to analyze YLD ability to regulate inflammatory factors and restore skin barrier proteins. Flow cytometry was additionally used to investigate YLD modulatory effects on type I, II, and III adaptive immune responses.

Results: YLD could inhibit the differentiation of macrophages into M1 phenotype in vitro. In the AD-like mice, YLD ameliorated epidermal hyperkeratosis and skin lesions, decreased the severity scoring of AD, and suppressed the inflammation of the skin in a dose-dependent manner. Moreover, YLD downregulated pro-inflammatory factors such as IL-4/13, TNF-α, TSLP, and IgE antibodies, restored the expression of barrier proteins in the skin, decreased the infiltration of CD4+ T cells in AD skin, and reestablished the balance of Th1/ Th2/ Th17 cells.

Conclusion: YLD alleviated AD by regulating the adaptive immune response through modulation of T cell differentiation and cytokine production, and by restoring skin barrier function. The study revealed the therapeutic mechanism of YLD and provided experimental evidence supporting its application in AD treatment.

Keywords: atopic dermatitis, Yin-hua Li-shi decoction, inflammatory factors, helper T cells, skin barrier function

Introduction

Atopic dermatitis (AD) is the most prevalent chronic and pruritic inflammatory skin disease,[1] characterized by epidermal desquamation, intense pruritus, and lichenified lesions.[2] This disease affects 20% of children and 4% of adults globally, causing significant quality-of-life impairment due to chronic pruritus, sleep disturbance, and psychosocial burden.[3,4] Common antigens triggering AD include house dust mites, *Staphylococcus aureus* enterotoxins, food allergens (eg, egg, milk), and environmental pollens.[5] AD is a continuous process from acute to chronic phase, accompanied by three interconnected pathological mechanisms, skin barrier dysfunction, immune dysregulation, and abnormal neural signaling.[6–8] Skin barrier dysfunction manifests as downregulated expression of barrier genes, such as loricrin (LOR), filaggrin (FLG), and elongation of very long-chain fatty acid (ELOVL).[9–11] Immune dysregulation mainly results from sustained inflammation mediated by type I, II, and III adaptive immune responses driven by

Received: 8 May 2025
Accepted: 23 August 2025
Published: 21 October 2025

differentiated CD4+ T cells (Th1/ Th2/ Th17).[12] Abnormal neural signaling manifests as sensory nerve hyperinnervation, upregulated pruritogens, such as interleukin (IL) −31 and thymic stromal lymphopoietin (TSLP), and neuroimmune crosstalk amplifying itch-scratch cycles.[13] These three components reinforce each other.[14] Environmental antigens first damage the skin barrier, which activates dendritic cells (DCs) and recruits Th cells. Activated Th cells release cytokines like IL-4, IL-13, and IL-31. These cytokines further break down barrier proteins and sensitize sensory nerves. Finally, neurogenic inflammation causes tissue damage which makes the immune system overactive, establishing a harmful cycle that worsens AD.[15]

For decades, the cornerstone of AD treatment has relied on topical corticosteroids and topical calcineurin inhibitors,[16] whose adverse effects include skin atrophy, pigmentation changes, anaphylaxis, and potential complications (eg, folliculitis or tinea infection) after drug discontinuation.[17] Recent advances in biological agents and small molecule inhibitors have introduced novel treatment options for AD, such as dupilumab (targeting IL-4Rα), tralokinumab/ lebrikizumab (targeting IL-13), CIM331/ nemolizumab (targeting IL-31R), crisaborole (targeting Phosphodiesterase-4), and tofacitinib (targeting Janus kinase 1/ 3).[18] At the same time, because of potential safety problems, high recurrence rate and high economic burden of the AD, the use of these drugs is limited. In this context, traditional Chinese medicine (TCM) has attracted the attention of clinicians and AD patients as a complementary treatment for AD, especially in and around China, due to its abundance of natural anti-inflammatory compounds.[19]

Yin-Hua Li-Shi Decoction (YLD) is a TCM approved by medical institutions, which is composed of six herbs aimed at removing dampness. It has a long history of being used for the treatment of AD. The chlorogenic acid and luteoloside derived from honeysuckle in YLD has been shown to inhibit the secretion of pro-inflammatory cytokines such as IL-6 and TSLP that acts on multiple cell lineages, including macrophages, mast cells, neutrophils, DCs, and T cells, ultimately suppressing moderate to severe immune responses.[20,21] However, the specific mechanisms underlying YLD in the treatment of AD were still unclear and lacked systematic validation.

The present study was aimed at exploring the therapeutic effects and mechanisms of YLD in AD. We used MC903-induced AD-like mouse model to evaluate YLD therapeutic benefits for AD and to clarify the mechanisms by which it regulated immunity and restored the skin barrier.

Material and Methods

Drugs and Reagents

All herbs were purchased from WanShiCheng Pharmaceutical Co., Ltd. (Shanghai, China), and authenticated according to the Pharmacopoeia of the People's Republic of China 2020 Edition by Professor Huijun Pan from Shanghai Skin Disease Hospital, School of Medicine, Tongji University. Voucher specimens of these herbal materials were deposited at the Shanghai Skin Disease Hospital with reference numbers YL1-6. Chlorogenic acid and specnuezhenide used as standard compounds were from Meilunbio (Shanghai, China). MC903 was purchased from Macklin Biochemical Co., Ltd. (#C833062, Shanghai, China). Antibodies used in the study were obtained from the following sources: anti-FLG (#GTX23137, GeneTex, Beijing, China), anti-LOR (#A21039, ABclonal, Wuhan, China), anti-ELOVL6 (#A21094, ABclonal, Wuhan, China), anti-TSLP (#ab188766, Abcam, Cambridge, U.K)., anti-β-Actin (#AC026, ABclonal, Wuhan, China), HRP-conjugated Goat anti-Rabbit IgG (H+L) (#AS014, ABclonal, Wuhan, China), anti-IL-4 (#25-7042-42, Invitrogen, California, USA), anti-IL-17A (#506904, Biolegend, California, USA), anti-IFN-γ (#563376, BD Biosciences, New Jersey, USA), anti-rabbit IgG (H+L) Ab HRP Affinity purified polyclonal (#95058–730, KPL, Maryland, USA), anti-CD4 (#ab183685, Abcam, Cambridge, U.K)., anti-CD4 (#555349, BD Biosciences, New Jersey, USA), anti-CD8 (#100733, Biolegend, California, USA), anti-CD86 and anti-CD80 (#561962 and #561955, BD Biosciences, New Jersey, USA). ELISA kits used for analysis were IL-4 (#EM3199M, WellBio, Shanghai, China), IL-13 (#EM3167M, WellBio, Shanghai, China), TNF-α (#RK00027, ABclonal, Wuhan, China), and IgE (#RK00170, ABclonal, Wuhan, China). Annexin V-FITC/PI Apoptosis Detection Kit was purchased from Vazyme Biotechnology Co., Ltd (#A211-02, Nanjing, China). All other chemicals used in the experiments were of analytical grade.

Preparation of YLD

The YLD consists of six Chinese herbal medicines, including Jinyinhua (Honeysuckle), Shanyao (Yam, Siberian), Huangjing (Solomonseal rhizome), Digupi (Cortex lycii radices), Nvzhenzi (Fructus ligustri lucidi), Yiyiren (Coix seed), and the daily dose of adult clinical YLD is 54 g of crude drugs (Table 1). YLD extraction is the first step to adding 8 times amount of water in crude drugs (w/w), decocting 2 h after filtering, the rest of the student to join six times the amount of water decoction 1 h again. The above water extract was concentrated to 40 mL using a EYELA N-1300D-WB rotary evaporator, and the final YLD concentration had a crude drug equivalent of 6.00 g/mL. The concentration was appropriately diluted to crude drug equivalents of 3.00 g/mL and 1.50 g/mL to form medium and low doses, respectively. All prepared YLD samples were stored at 4 °C until subsequent use.

Quality Control of YLD

Fingerprint Identification

High-performance liquid chromatography (HPLC) was employed to construct a fingerprint profile and evaluate the quality of YLD and for quality control. Chlorogenic acid and specnuezhenide were dissolved in methanol to prepare a stock solution. The YLD reference solution (R) (200 μg/mL) was prepared by diluting the original 1.50 g/mL YLD solution and then filtering through a 0.45 μm membrane filter. The concentration of YLD extract (g crude herb/mL) represented a drug extract ratio, which was calculated by the quotient of total dry herb mass over final decoction volume.[22] The YLD HPLC test solution (YLD sample) (150 μg/mL) was prepared by diluting the original 1.50 g/mL YLD solution and then filtering through a 0.45 μm membrane filter. The quality consistency validation and methodological parameters are detailed in Supplementary Information 1 Table S1. The content of the reference compounds in YLD was calculated based on the pre-constructed standard curves of chlorogenic acid and specnuezhenide. The fingerprint profile of YLD was identified by comparing the relative retention time and ultraviolet characteristics of the internal reference with the YLD test sample. The quality of YLD was controlled by comparing the similarity of the fingerprint profiles among 10 batches of YLD (S1-S10). To ensure batch consistency, all 10 tested batches were derived from the same cultivation batch of raw plants.

The liquid chromatography system used was an Waters Alliance HPLC (Waters, Massachusetts, USA), consisting of an E2695 separation module and a 2998 photodiode array detector with an autosampler. HPLC was performed on an ZORBAX Eclipse Plus C18 column (4.6 mm × 250 mm, 5 μm) (Agilent, California, USA). The mobile phase consisted of solvent A (acetonitrile) and solvent B (0.1% phosphoric acid water), and the gradient elution conditions were shown in Table 2. The UV absorption wavelength was set at 230 nm, column temperature at 25 °C, injection volume at 10 μL, and flow rate at 1.0 mL/min.

Ingredient Identification

The components of YLD water extract were identified by liquid chromatography-tandem mass spectrometry (LC-MS). The YLD LC-MS test solution (600 μg/mL) was prepared by diluting the original 1.50 g/mL YLD solution and then filtering through a 0.45 μm membrane filter. The YLD water extract was analyzed using a LC-MS system composed of an ACQUITY UPLC I-Class HF ultra-high performance liquid chromatography coupled with a QE high-resolution mass

Table 1 The Herbal Composition of YLD

Latin Name	English Name	Chinese Name	Plant Part	Amount (g)*
Lonicera japonica Thunb.	Honeysuckle	Jinyinhua	Flower	9
Dioscorea opposita Thunb.	Yam	Shanyao	Root	9
Polygonatum sibiricum Red	Siberian Solomonseal rhizome	Huangjing	Root	9
Lycium barbarum L.	Cortex lycii radicis	Digupi	Root	9
Ligustrum lucidum Ait.	Fructus ligustri lucidi	Nvzhenzi	Fructus	9
Coix lacryma-jobi L.	Coix seed	Yiyiren	Species	9

Notes: * The mass of the 6 herbs contained in the daily dose of YLD for clinical use by adults.

https://doi.org/10.2147/JIR.S531656

Table 2 HPLC Gradient Evaluation Conditions of YLD

Time (Minutes)	Acetonitrile (%)	0.1% Phosphoric Acid Water (%)
0	0	0
5	10	90
10	20	80
30	33	67
35	100	0
40	100	0

spectrometer. The mobile phase consisted of solvent A (0.1% formic acid aqueous solution) and solvent B (acetonitrile). The sample was separated at a flow rate of 0.35 mL/min, and the gradient elution conditions are shown in Table 3.

LC-MS detection was performed using an ACQUITY UPLC HSS T3 column (100 mm × 2.1 mm, 1.8 μm) (Waters, Massachusetts, USA). Mass spectrometry data acquisition was carried out in electrospray ionization (ESI) positive and negative modes, and the data-dependent acquisition (DDA) mode was used, with a mass range of m/z 90 to 1300. The capillary temperature was set to 320 °C, and the probe heating temperature was set to 350 °C.

Cell Culture

Murine macrophage cell line (RAW264.7) and human keratinocyte cell line (HaCaT) were obtained from the National Collection of Authenticated Cell Cultures (Shanghai, China). RAW264.7 and HaCaT cells were cultured in DMEM (Gibco, USA) supplemented with 10% FBS (Gibco, USA) and 1% penicillin-streptomycin (Beyotime, China). All cultures were maintained in a humidified atmosphere with 5% CO_2 at 37 °C.

Animals

Male BALB/c mice aged 8–9 weeks (weighing 22–25 g) were obtained from the SiPeiFu Biotechnology Co., Ltd. (Shanghai, China) and housed under SPF conditions. The mice were maintained at a room temperature of 26 °C with a relative humidity of 40% and a 12:12-hour light/dark cycle. They were provided with standard mouse maintenance feed and water ad libitum.

Apoptosis Assay

HaCaT cells were cultured in 6-well plates (30×10^4 cells per well) for 24 h. The 6-well plate was then subjected to a 24-hour incubation in the following groups: the PBS group (0 μg/mL YLD) and the PBS+YLD group (150 μg/mL YLD). Apoptosis of HaCaT cells was assessed using propidium iodide (PI) and fluorescein isothiocyanate (FITC)-labeled Annexin V staining, followed by detection and analysis with Navios 6 COLORS/2 LASER flow cytometer and FlowJo Software.

Table 3 LC-MS Gradient Elution Conditions of YLD

Time (Minutes)	Acetonitrile (%)	0.1% Phosphoric Acid Water (%)
0	95	5
2	95	5
4	70	30
8	50	50
10	20	80
14	0	100
15	0	100
15.1	95	5
16	95	5

Analysis of Macrophage Phenotype

To induce the inflammatory phenotype of macrophages, RAW264.7 cells were treated with 0.5 μg/mL LPS and 2 ng/mL IFN-γ. 1 h prior to LPS and IFN-γ stimulation, RAW264.7 cells were treated with YLD (150 μg/mL) to assess the impact of YLD on macrophages. After 18 h, cells were incubated with CD86 and CD80 antibodies for 30 minutes. The Navios 6 COLORS/2 LASER flow cytometer and FlowJo software were used to evaluate the differentiation of YLD in suppressing the inflammatory phenotype of macrophages.

Induction of AD-Like Mice Model and YLD Administration

Fifty male BALB/c mice were induced with AD by repeated topical application of MC903 on their ears for 14 days. The mice were randomly divided into five groups (n = 10/group): control mice treated with ethanol (Ethanol), control mice treated with MC903 alone (MC903), experimental mice treated with both MC903 and low-dose YLD (YLD-L), experimental mice treated with both MC903 and medium-dose YLD (YLD-M), and experimental mice treated with both MC903 and high-dose YLD (YLD-H). In brief, Ethanol group was topically applied with 20 μL of ethanol on the ears daily, while other groups were sensitized with 2 nmol of MC903 on the ears daily for 15 days (Day 0 to Day 14). From Day 1 to Day 14, Ethanol group received daily treatment with ethanol, and YLD-treated groups received oral administration after diluting YLD extract. Three different dosage levels were used: low, medium, and high, corresponding to final concentrations of 1.50 g/mL, 3.00 g/mL, and 6.00 g/mL of the YLD extract, respectively. The lose dose was calculated based on the clinical dose converted to mouse dose referring to the FDA human dose conversion table for animal doses. And each 20 g mouse received 0.15 mL decoction orally daily. The efficacy of the treatment was evaluated 12 h after the last administration (Day 15). Blood samples were collected by retro-orbital bleeding to obtain serum samples, and tissue samples were collected after cervical dislocation for subsequent experimental analysis.

AD-Related Evaluation

During the study, daily monitoring of mice included recording body weight using an electronic balance, measuring transepidermal water loss (TEWL) using an intelligent skin analyzer (#W-2100, Yizi-moqi, Guangzhou, China), assessing ear thickness using vernier calipers, and scoring AD (SCORAD). The SCORAD consisted of the following items: (i) pruritus/itching, (ii) erythema/hemorrhage, (iii) edema, (iv) excoriation/erosion, and (v) desquamation/dryness. Each symptom was graded as follows: 0 (no symptoms), 1 (mild), 2 (moderate), or 3 (severe). The total score for AD ranged from 0 to 15. Additionally, spleen index was measured on Day 15. The spleen index was calculated using the formula:

Spleen Index (mg/g) = Spleen weight (mg) /Mouse weight (g).

Histopathological Analysis

Tissue specimens from the inflamed area of the ear were fixed in formalin and embedded in paraffin. For hematoxylin and eosin (HE) staining, paraffin sections were stained with hematoxylin and eosin. Samples were examined and captured using an optical microscope (QT50GS, Yuehe, Shanghai, China), and the epidermal thickness was counted at five randomly selected sites under 40× and 100× magnification. For toluidine blue (TB) staining, paraffin sections were stained with TB. Samples were examined and captured using an optical microscope, and the number of mast cells was counted at five randomly selected sites under 40× magnification.

Enzyme-Linked Immunosorbent Assay (ELISA)

Mouse blood samples were centrifuged at 12,000 g and 4 °C for 20 minutes to separate the upper serum. ELISA was performed to measure the concentrations of IL-4, IL-13, TNF-α, and IgE in the serum. The measurements were carried out using commercially available ELISA kits following the manufacturer's instructions.

Immunohistochemical Analysis

Paraffin-embedded tissue specimens were incubated overnight with anti-FLG (1:500), anti-TSLP (1:500), and anti-CD4 (1:500). After washing with PBS, Anti-Rabbit IgG (H+L) Ab HRP Affinity purified polyclonal (1:200) were added and

incubated for 1 h, followed by DAB staining. The sections were counterstained with hematoxylin. Immunohistochemically stained slides were examined and captured using an optical microscope, and records were taken at five randomly selected sites under 40× magnification.

Western Blot Analysis

Tissue protein lysates were obtained in RIPA buffer (Beyotime, Shanghai, China) containing PMSF (Beyotime, Shanghai, China). Protein concentration was quantified using a BCA assay kit (Beyotime, Shanghai, China). Proteins were separated by 10% SDS-PAGE (Servicebio, Wuhan, China) and then transferred onto PVDF membranes. The membranes were incubated overnight at 4 °C with corresponding primary antibodies: anti-FLG, anti-LOR, anti-ELOVL6, anti-TSLP (1:1000), and anti-β-Actin (1:2000). Subsequently, the membranes were incubated with secondary HRP-conjugated (1:1000) for 1 h to detect antibody binding. β-Actin was used as an internal reference. The target protein signals were analyzed using Image J application.

Analysis of Spleen T Cells

Spleen tissue was dissociated and filtered through a 70 μm cell strainer. The cell suspension was centrifuged, and resuspended in PBS to prepare a single-cell suspension. Red blood cells in the splenocytes were removed using ACK lysis buffer (#A1049201, Thermo Fisher Scientific, Massachusetts, USA) and washed before staining. Cells were incubated at 4 °C in the dark for 30 minutes with 2.5 μL of CD4 antibody and CD8 antibody. Subsequently, a permeabilization wash buffer was added. Then, 2.5 μL of IL-4, IFN-γ, and IL-17A antibodies were added, and the cells were incubated at 4 °C for 30 minutes. The analysis was performed using a Beckman moflo Astrios EQ flow cytometer with FlowJo Software, and the proportions of Th1, Th2, and Th17 cells in CD4+ T cells were recorded.

Statistical Analysis

Data analysis and graph plotting were performed using GraphPad software (version 8.0). Normality of data distribution was verified using the Shapiro–Wilk test (α=0.05). Normally distributed data were analyzed by one-way ANOVA with Tukey's post hoc test. Data were expressed as mean ± standard deviation (SD), and one-way ANOVA was used for comparisons among multiple groups. A P-value < 0.05 was considered statistically significant.

Results

Fingerprint and Component Identification of YLD

To ensure the stability of YLD, chlorogenic acid and specnuezhenide were selected as reference compounds and studied as specific indicators of YLD (Figure 1A). HPLC analysis was performed on the reference compounds, with a retention time of 12.7 minutes for chlorogenic acid and 26.3 minutes for specnuezhenide. The peak shape of both chlorogenic acid and specnuezhenide exhibited Gaussian distribution, with sharp and symmetrical peaks.

The standard curves of chlorogenic acid and specnuezhenide reference compounds were provided in the Supplementary Information 1 Tables S2 and S3, Figure S1a and b). Based on the standard curves of these two reference compounds, the content of chlorogenic acid in YLD (clinical) was determined to be 2.697 mg/mL and the content of specnuezhenide was determined to be 8.405 mg/mL. We conducted fingerprint analysis of YLD from 10 batches (Figure 1B), and the highest similarity exceeded 0.9006 (Supplementary Information 1 Table S4). The above analysis data indicated that YLD was stable and of controllable quality.

The chemical components of the YLD extract included a total of 705 compound molecules, which were identified using LC-MS. These 705 compounds were classified chemically based on their quantity and content, as shown in Figure 1C. The Base Peak Chromatogram (BPC) in both positive and negative ion modes is presented in Figure 1D. The top 15 most abundant compounds among the 705 metabolites identified are Secologanic acid, Citric acid, Cryptochlorogenic acid, GL3, Specnuezhenide, Secoxyloganin, Mannoheptulose, Sucrose, Turanose, Swertiamarin, D-Galactose, Verbenalol, Dambose, 5-Hydroxymethylfurfural, 6α-dihydrocornic acid, and Salidroside (Table 4). The quantitative and qualitative identification results of the 705 metabolites in the YLD extract are provided in the Supplementary Information 2.

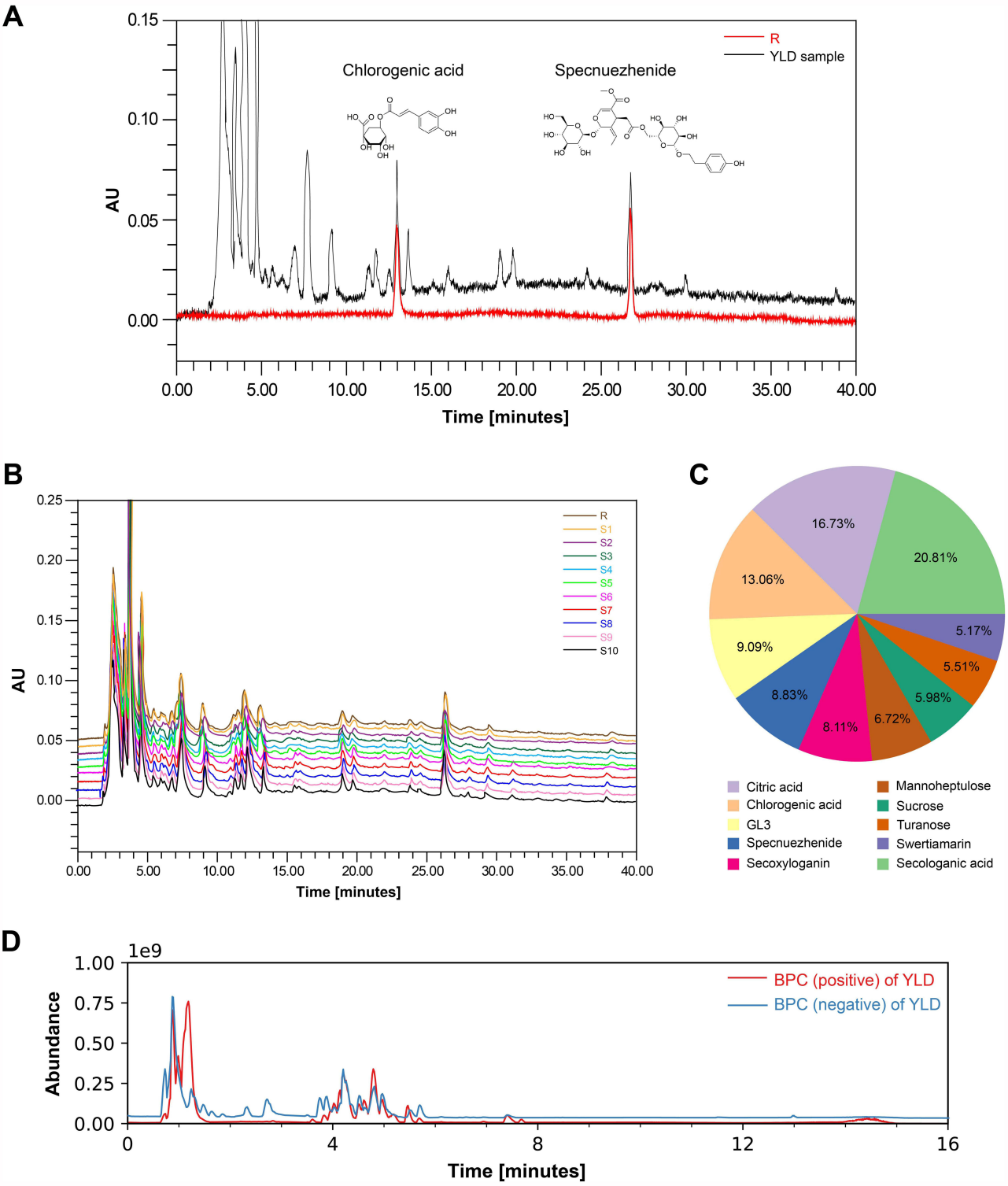

Figure 1 HPLC fingerprint of YLD. Chromatogram at 230 nm showing the reference compounds and the chromatogram (**A**), and fingerprints of ten different batches (**B**) of YLD. (**C**) Distribution chart of the top 10 components in terms of content in YLD. (**D**) BPC chromatograms of YLD in positive and negative ion modes.

YLD Did Not Induce Apoptosis in HaCaT

Flow cytometry, utilizing PI and membrane-associated protein V-FITC staining, was employed to assess the impact of YLD on apoptosis in HaCaT. After treatment with 150 μg/mL of YLD for 24 h, there was an increase in the percentage of apoptotic HaCaT but was no significant difference (Figure 2A). However, the viability of HaCaT remained above

https://doi.org/10.2147/JIR.S531656

Table 4 Top 15 Most Abundant Compounds Among YLD Metabolites

No.	ID	Metabolites	Adducts	Formula	m/z	Theoretical m/z	Retention Time (min)	Ion Mode	TCM Mean Value	TCM Mean Value (Percentage of Peak Area Ratio)
1	4.27_374.1215n	Secologanic acid	M-H, M+FA-H, 2M-H	C16H22O10	747.23582	747.2353	4.2653	NEG	36994368.6	11.69005
2	1.18_191.0197m/z	Citric acid	M-H	C6H8O7	191.019656	191.0197	1.184833333	NEG	29726588.2	9.393467
3	4.20_353.0874m/z	Cryptochlorogenic acid	M-H	C16H18O9	353.087403	353.0878	4.199433333	NEG	23204251	7.332438
4	5.51_1117.3621m/z	GL3	M+FA-H	C48H64O27	1117.36213	1117.3617	5.507033333	NEG	16151462.7	5.103789
5	4.96_686.2422n	Specnuezhenide	M+H-H2O, M+NH4, M+K, M+H	C31H42O17	704.276008	704.276	4.95725	POS	15695354	4.95966
6	4.61_403.1244m/z	Secoxyloganin	M-H	C17H24O11	403.124367	403.1246	4.606383333	NEG	14419156.6	4.556388
7	0.87_191.0559m/z	Mannoheptulose	M-H2O-H	C7H14O7	191.055904	191.0561	0.866966667	NEG	11937115.5	3.772074
8	0.92_342.1153n	Sucrose	M+NH4, M+Na, M+H, M+H-H2O	C12H22O11	365.104484	365.1055	0.916816667	POS	10630297.7	3.359126
9	0.83_342.1158n	Turanose	M-H, M+FA-H	C12H22O11	387.113965	387.1145	0.83105	NEG	9789200.59	3.093343
10	4.25_374.1205n	Swertiamarin	M+H, M+K, M+Na, M+NH4, M+H-H2O	C16H22O10	397.109674	397.1106	4.249266667	POS	9181812.1	2.901411
11	0.82_180.0633n	D-Galactose	M-H2O-H, M-H, M+FA-H	C6H12O6	179.05604	179.0561	0.817166667	NEG	6214655.76	1.963803
12	4.80_226.0839n	Verbenalol	M+H-H2O, M+H	C11H14O5	227.091155	227.0914	4.801	POS	5374679.27	1.698374
13	0.84_219.0264m/z	Dambose	M+K	C6H12O6	219.026355	219.0266	0.843066667	POS	4510119.66	1.425177
14	2.71_126.0318n	5-Hydroxymethylfurfural	M+H-H2O, M+H	C6H6O3	127.039089	127.039	2.711733333	POS	4178453.31	1.320372
15	3.96_375.1293m/z	6α-dihydrocornicacid	M-H	C16H24O10	375.129316	375.1297	3.960116667	NEG	3876761.69	1.225039

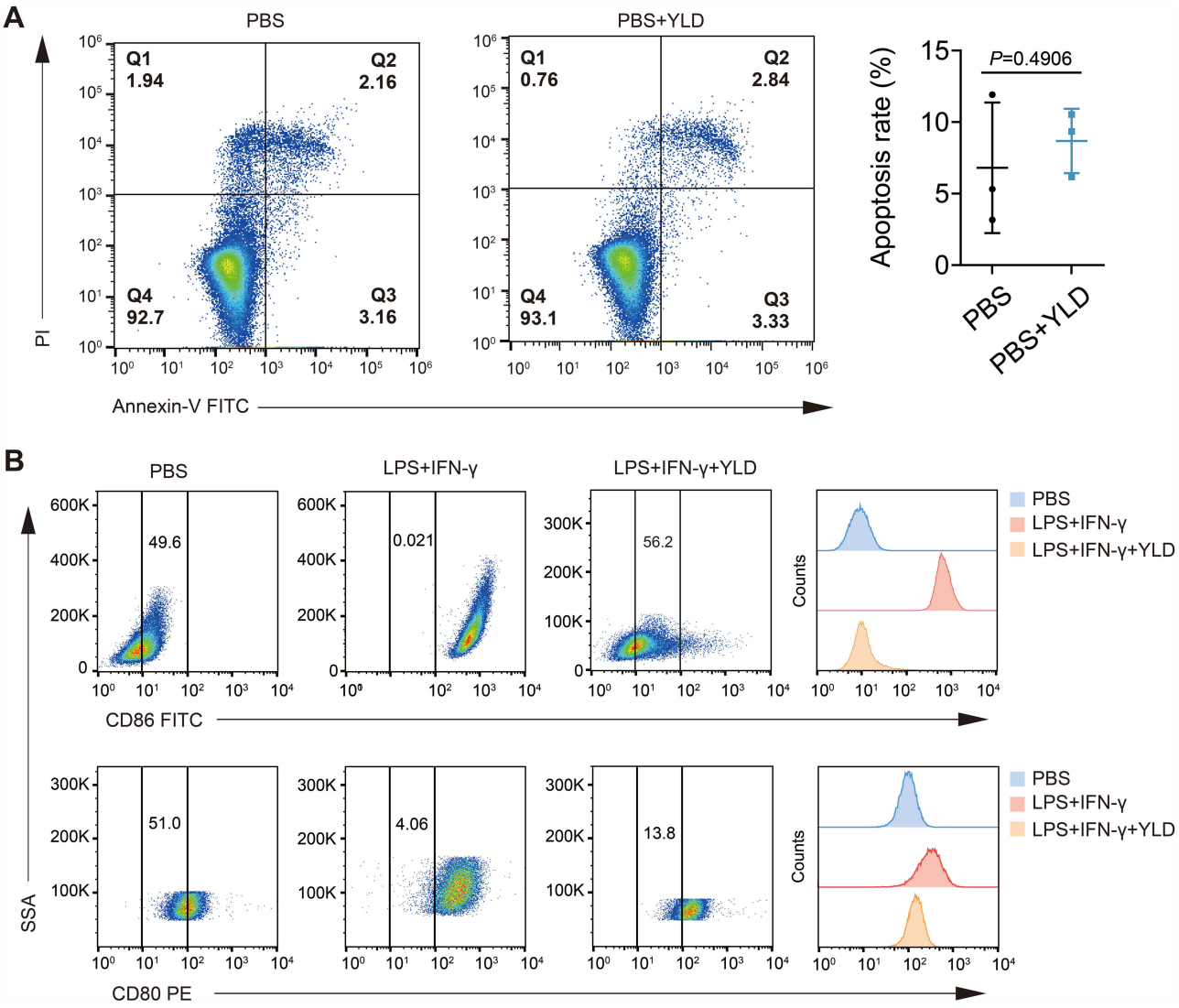

Figure 2 In vitro pharmacological activity of YLD. (**A**) Apoptotic HaCaT treated with 150 μg/mL YLD for 24 h were detected by flow cytometry. (**B**) M1 macrophages were treated with YLD (150 μg/mL) for 24 h and then detected the M1-phenotype surface marker (CD86 and CD80) by flow cytometry. The data was collected from three independent experiments and was presented as a mean ± SD.

80%. Generally, a cell survival rate greater than 80% post-drug treatment is considered indicative that the drug does not induce apoptosis.

YLD Inhibited Macrophage to M1 Differentiation

Macrophages, essential phagocytic cells of the immune system, play a crucial role in coordinating innate immune responses.[23] It is noteworthy that macrophages also possess antigen-presenting capabilities, facilitating the presentation of antigen peptides to T cells, thereby initiating adaptive immune responses.[24] M1 macrophages represent classically activated macrophages that exhibit a pro-inflammatory phenotype, characterized by the production of high levels of cytokines such as IL-1β, IL-6, and TNF-α.[25]

Stimulation of RAW264.7 with 0.5 μg/mL LPS and 2 ng/mL IFN-γ for 24 h induced the differentiation of macrophages into the M1 subtype. CD86 and CD80 are widely used as markers for M1 polarization, with their upregulation considered indicative of activated macrophages polarizing towards the M1 phenotype. Examination of M1 macrophages stimulated by LPS and IFN-γ revealed higher expression of the specific functional markers CD86 and CD80, suggesting the induction of M0 differentiation into M1. In comparison to the LPS + IFN-γ group, YLD treatment

https://doi.org/10.2147/JIR.S531656

for 24 h significantly downregulated the positivity rates of CD86 and CD80, which indicated that YLD possessed the capability to inhibit the differentiation of macrophages into the inflammatory phenotype (Figure 2B).

YLD Alleviated Clinical Symptoms of MC903-Induced AD in Mice

The experimental design for the model construction in this study was shown in Figure 3A. MC903 is a vitamin D3 analog that has been widely used as an experimental drug for establishing AD animal models.[26] Under the stimulation of MC903, keratinocytes in mouse skin express and secrete TSLP, which induces the development of immature DCs to a mature phenotype by binding to TSLP receptors on DCs.[27,28] The activated DCs further initiate the differentiation of naive Th0 cells into Th2 subsets, thereby inducing Th2-mediated inflammatory response, down-regulating the expression of skin barrier related proteins, and promoting the production of allergen-specific IgE by B cells.[29] Thus, the mechanism by which MC903 induces AD-like skin lesions is similar to the pathogenesis of human AD.[30]

Compared to the ethanol group, continuous stimulation with MC903 resulted in typical AD symptoms, significant ear epidermal swelling, erythema, and crust formation in mice (Figure 3B). The SCORAD, used to evaluate the severity of skin lesions in the MC903 group, reached 8.50 (Figure 3C). However, the YLD-M and YLD-H groups shown significantly reduced severity of skin damage compared to the MC903 group, with SCORAD of 6.08 and 6.62, respectively. Additionally, AD caused a decrease in body weight in the MC903 group, which was improved after oral administration of YLD. The YLD-M group exhibited the best control of body weight (Figure 3D). Moreover, while both the YLD-M and YLD-H groups shown therapeutic effects, it was observed that the YLD-H group caused adverse reactions in the gastrointestinal tract of AD-like mice.

Comparing the dynamic changes in TEWL in the lesional skin of mice in each group during YLD treatment, the results showed that the TEWL of mice in the MC903 group continued to increase under the action of MC903. There were significant differences between the MC903 group and other groups. After YLD treatment, TEWL in AD mice was significantly down-regulated, but there was no significant difference in TEWL between gradient YLD treatment groups (Figure 3E). AD-like mice's ear thickness changes due to ear swelling during YLD treatment were statistically analyzed. Prolonged stimulation with MC903 resulted in significant ear swelling in mice, with an average change rate in ear thickness of 40.61% in the MC903 group at the end of AD induction. However, the average change rate in ear thickness was 25.24% in the YLD-L group, 23.17% in the YLD-M group, and 17.49% in the YLD-H group (Figure 3F), which was weaker than the counterpart in the MC903 group.

YLD Ameliorated Skin Lesions in AD Mice

HE staining was used to compare the epidermal lesions in the ears of AD-like mice and the YLD-treated groups. Compared to healthy ears, MC903-induced AD-like ears exhibited apparent hyperkeratosis (with a thickness of up to 95.36), incomplete keratinization, thickened spinous layers, increased granular layer, and infiltration of numerous inflammatory cells and eosinophils in the dermis (Figure 4A). The epidermal thickness in healthy mice was 36.31. In the YLD-L group, the epidermal thickness in mice could be reduced to 71.01. However, results shown that the mice in the YLD-M and YLD-H groups gradually reduced these skin lesion symptoms and decreased epidermal thickness (69.7 in the YLD-M group and 62.52 in the YLD-H group). From the perspective of epidermal thickness, the therapeutic effects of YLD-L, YLD-M, and YLD-H in AD-like mice demonstrated a dose-dependent pattern.

TB staining was used to process ear specimens for counting classical immune sentinel mast cells to compare the number of inflammatory cells in the ears of AD-like mice and the YLD-treated groups. Mast cells are considered classical immune cells implicated in itch sensation, and their excessive infiltration can directly contribute to itching behavior in AD-like mice. By comparing sections from the blank group and AD-like skin, it was observed that the infiltration of mast cells in the dermis and subcutaneous tissue of AD-like mice significantly increased, surpassing the levels in healthy mice. However, in AD-like mice administered YLD orally, the infiltration of mast cells in the dermis and subcutaneous tissue decreased, and this reduction exhibited a correlation with the dosage (Figure 4B).

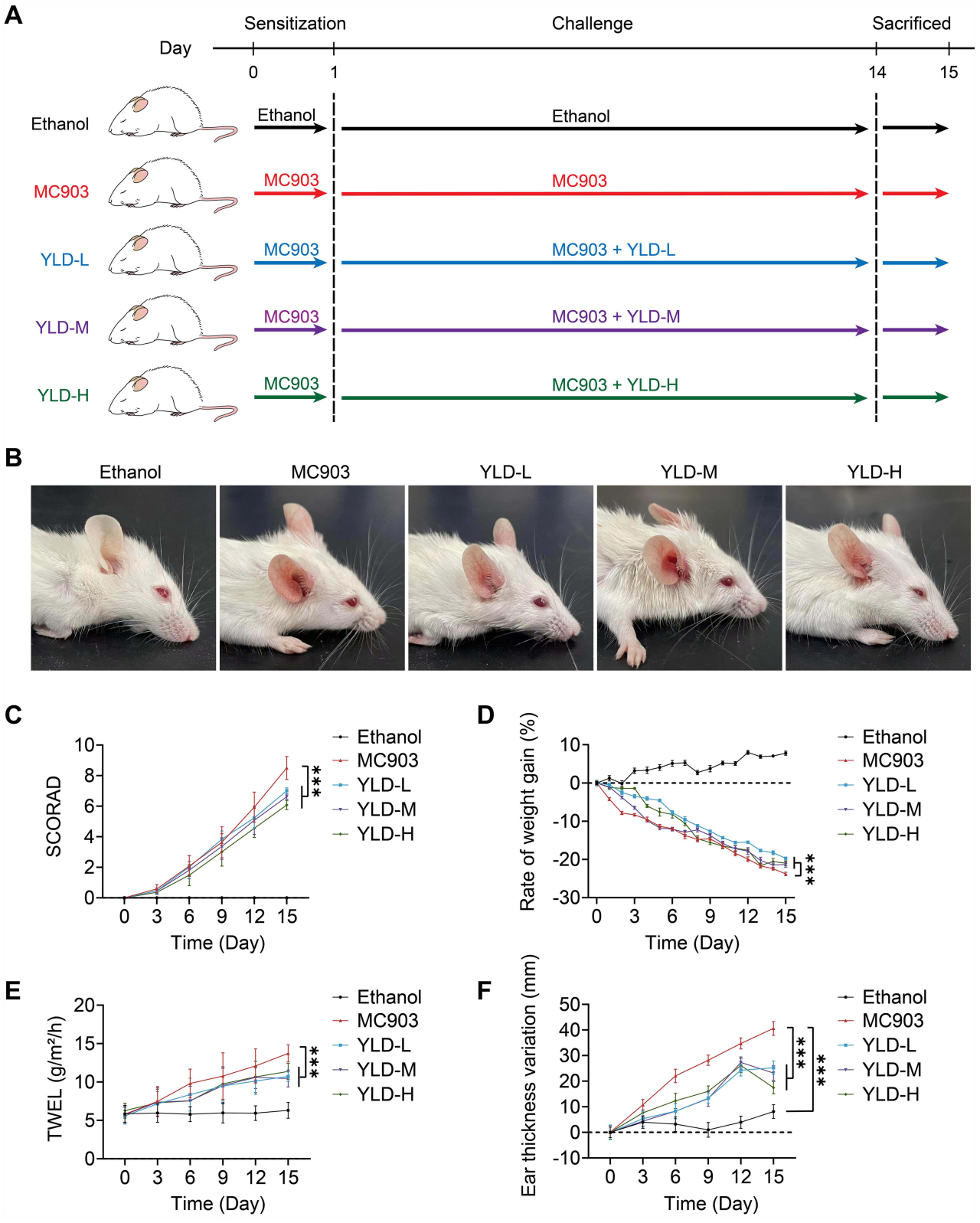

Figure 3 Improvement of AD symptoms in mice by YLD. (**A**) Schematic representation of the construction of the AD animal model and treatment regimen: BALB/c mice aged 9 weeks were administered MC903 at a dose of 2 nmol/ear for 15 consecutive days, followed by treatment with 0.2 mL of YLD-L, YLD-M, or YLD-H for 14 days. (**B**) Visual images/representative phenotypic manifestations of the ears of mice from the Ethanol group, MC903 group, YLD-L group, YLD-M group, and YLD-H group on day 15 of AD induction. (**C**) Daily SCORAD during YLD treatment. (**D**) Daily percentage change in body weight of mice during YLD treatment. (**E**) The TEWL of AD-like mice during YLD treatment. (**F**) Percentage change in ear thickness of mice during YLD treatment measured using a micrometer. Data were expressed as mean ± SD (n = 10 for each group). ***$P < 0.001$.

https://doi.org/10.2147/JIR.S531656

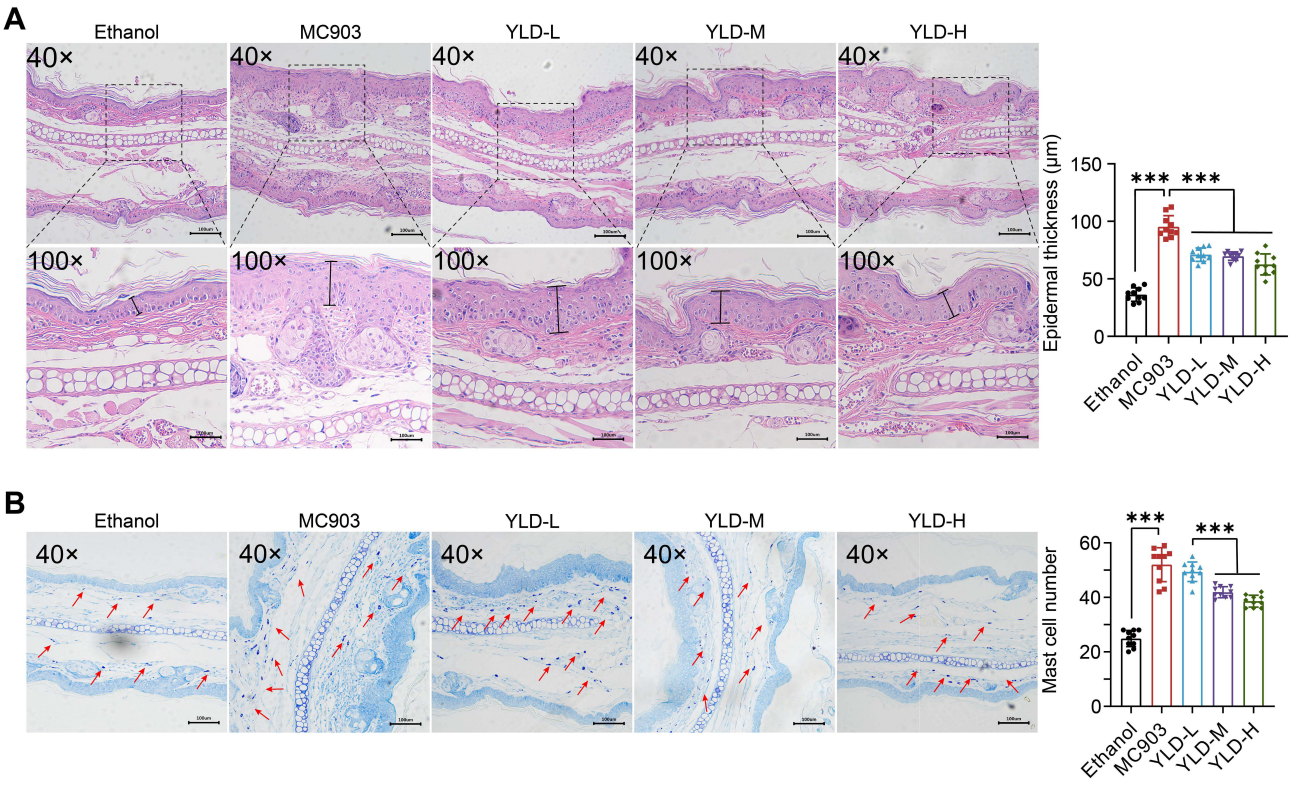

Figure 4 Improvement of skin lesions in AD-like mice by YLD. (**A**) HE staining of longitudinal cross-sections of ears and quantification histogram of stratum corneum thickness within the field of view. A solid black line represented the stratum corneum. Scale bar represented 100 μm. **(B)** TB staining of longitudinal cross-sections of ears and quantification histogram of mast cell infiltration within the field of view. Red arrows indicated mast cells. Scale bar represented 100 μm. Data were expressed as mean ± SD (n = 10 for each group). ***$P < 0.001$.

YLD Suppressed Pro-Inflammatory Cytokines in Serum

To evaluate the inflammatory status of mice, the concentrations of pro-inflammatory cytokines and an antibody in collected serum samples were measured using ELISA. Treatment with MC903 increased levels of IL-4, IL-13, TNF-α cytokines, and IgE antibodies in the serum (Figure 5A). However, YLD reduced the serum levels of these pro-inflammatory factors in AD-like mice. Mainly, in the YLD-H group, the mice shown a decrease of 49% in IL-4, 38% in IL-13, 38% in TNF-α, and 35% in IgE.

YLD Upregulated Barrier Proteins and Downregulated Pro-Inflammatory Factors in Lesional Skin

Previous studies indicated that AD lesional skin exhibits defects or downregulation of FLG, LOR, and ELOVL barrier proteins. To investigate the role of YLD in improving the downregulation of barrier proteins in AD-affected skin, western blot analysis was performed to examine the expression levels of barrier proteins. As shown in Figure 5B, the expression of FLG, LOR, and ELOVL was downregulated in the skin of mice treated with MC903, consistent with impaired barrier function in AD skin. However, in mice treated with YLD, the expression of FLG, LOR, and ELOVL increased, with the most significant upregulation observed in the YLD-H group. YLD also exhibited a typical downregulation effect on the pro-inflammatory cytokine TSLP. These protein expression assessments suggested that the anti-AD results of YLD were achieved by upregulating barrier protein expression and downregulating inflammatory factors.

Furthermore, the expression of FLG and TSLP in the skin was visually observed using immunohistochemistry (Figure 5C). Under continuous stimulation by MC903, the expression level of FLG in mice significantly decreased while TSLP expression increased. After YLD treatment, the expression level of FLG in AD lesional tissues recovered, and the highly expressed level of TSLP was controlled. These results were consistent with the findings from the western blot.

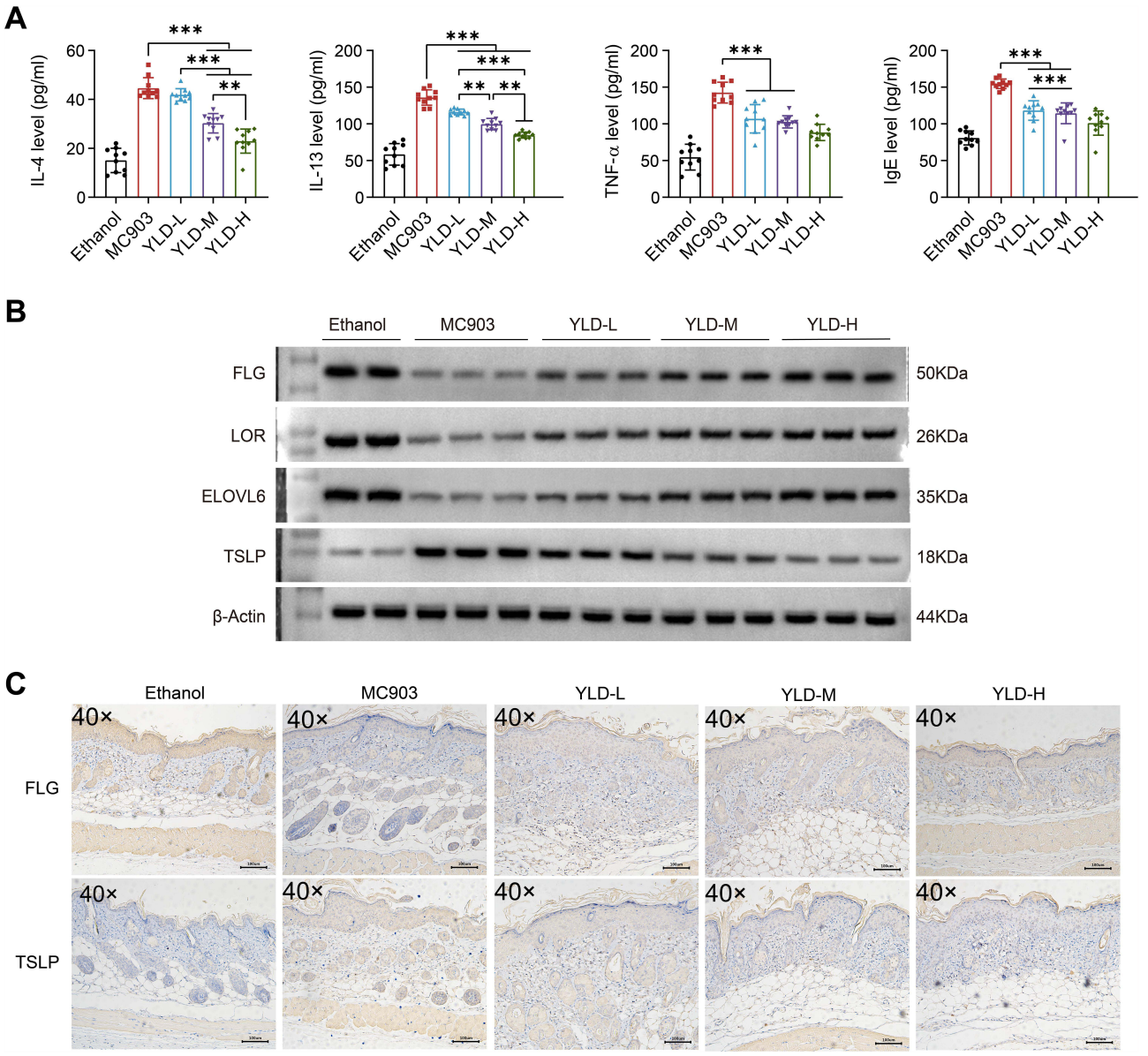

Figure 5 YLD alleviated AD by maintaining barrier protein expression and inhibiting pro-inflammatory factors. (**A**) Serum ELISA results shown that YLD downregulated the levels of typical pro-inflammatory factors IL-4/13, TNF-α, and IgE antibodies in AD-like mice, exhibiting a dose-dependent relationship. (**B**) Western blot results of AD-like skin lesions demonstrated that compared to MC903, YLD maintained the expression of typical barrier proteins FLG, LOR, and ELOVL6 in the skin lesions of mice with AD-like symptoms, with a dose-dependent effect observed for LOR and ELOVL6. Furthermore, compared to MC903, YLD downregulated the expression of pro-inflammatory factor TSLP in the skin lesions of AD-like mice. (**C**) Immunohistochemistry results of AD-like skin lesions shown that YLD maintained the expression of barrier protein FLG and inhibited the expression of pro-inflammatory factor TSLP, with a dose-dependent effect observed for the inhibition of TSLP. Scale bar represented 100 μm. Data were expressed as mean ± SD (n = 10 for each group). $^{**}P < 0.01$, $^{***}P < 0.001$.

However, in immunohistochemistry, dose-dependency was primarily reflected in FLG, and no obvious dose-dependency was observed for TSLP.

YLD Inhibited Splenic Atopic Immune Responses

To elucidate the mechanisms by which YLD regulated immune responses, immunohistochemistry analysis was used to analyze the infiltration of CD4+ T cells in lesional tissues and flow cytometry was used to analyze the quantity and proportion of Th1/ Th2/ Th17 immune cells in the spleens of mice from different treatment groups, aiming to characterize the regulation of YLD on CD4+ T cell subsets in AD-like mice. Compared to the skin tissue of healthy mice, CD4+ T cell infiltration in the epidermis of AD lesional skin significantly increased, indicating severe adaptive immune

https://doi.org/10.2147/JIR.S531656

responses induced by MC903 (Figure 6A). After YLD-L, YLD-M, and YLD-H treatments, a gradient reduction in infiltrating CD4+ T cells in the epidermis and dermis was observed, showing a correlation with the dosage. In the YLD-H treatment, the infiltration of CD4+ T cells in lesional areas approached levels seen in normal skin. As a typical immune organ, the spleen exhibited morphological changes indicative of AD-like immune responses, such as volume reduction. The number of immune cells in the spleen can represent the degree of immune responses. Morphologically, the spleen shown different degrees of shrinkage after treatment with MC903. However, YLD treatment attenuated the degree of spleen shrinkage (Figure 6B). Significant differences were observed in the spleens of the YLD-L and YLD-H groups compared to the MC903 group, which was also reflected in the spleen index.

Flow cytometry results shown that the proportions of CD4+ T, CD8+ T cells, and Th1, Th2, and Th17 cells in the spleens of AD-like mice significantly increased (Figure 7). Compared to healthy mice, the proportions of Th1, Th2, and Th17 cells in AD-like mice approximately doubled, representing the occurrence of type I, II, and III adaptive immune

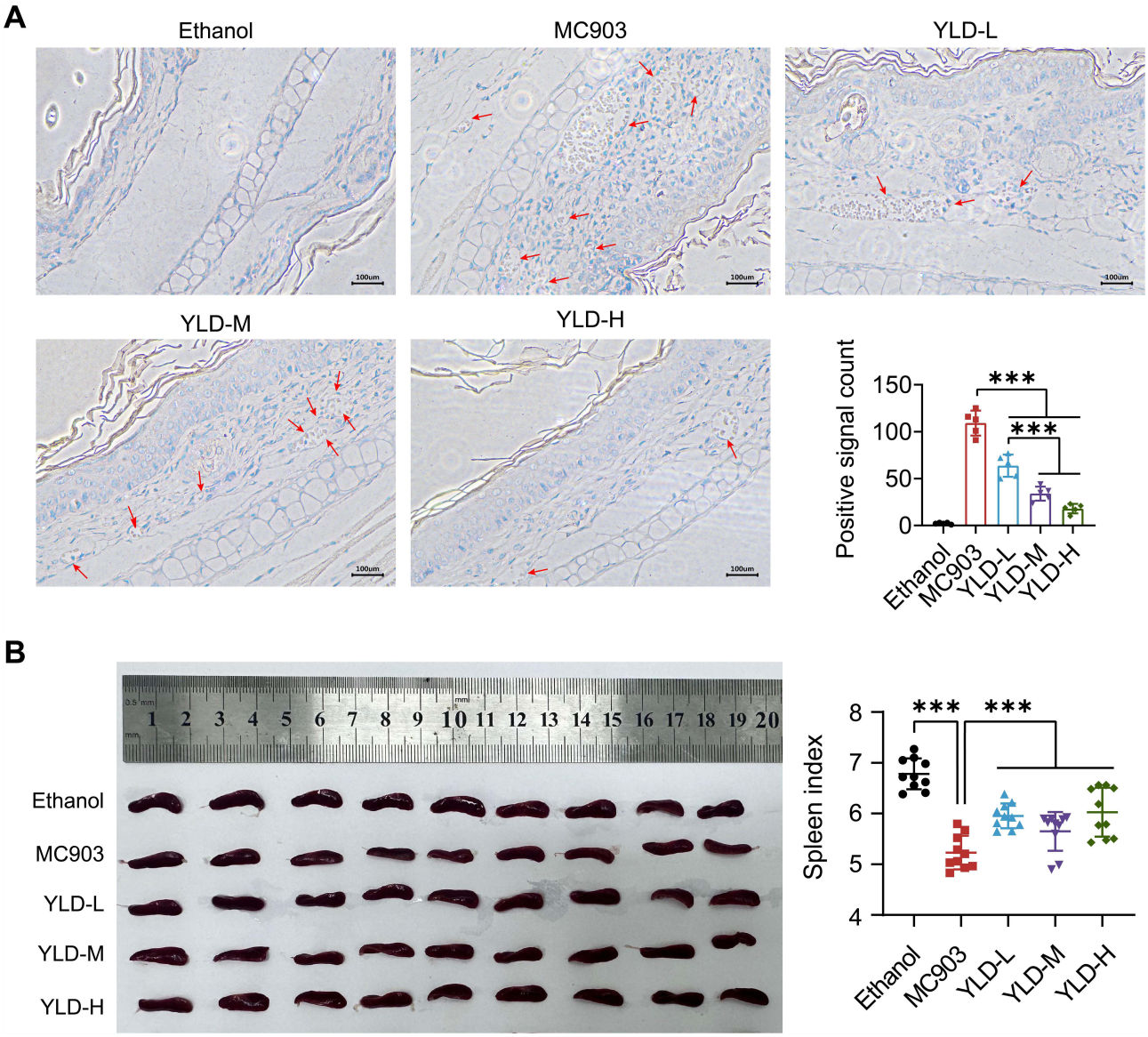

Figure 6 YLD exerted therapeutic effects in AD by inhibiting the activation of immune cells in the lesional skin. (**A**) Immunohistochemistry results shown a significant reduction in CD4+ T cell infiltrates in mice epidermis and dermis of the lesional skin after YLD treatment, compared to MC903. A slight dose-dependent relationship was observed among the three doses of YLD treatment. Red arrows indicated positive signal CD4+ T cells. (**B**) YLD inhibited splenic atopic immune responses, improved the typical atopic symptom of spleen shrinkage in AD-like mice, and restored the spleen index. Among the different doses of YLD treatment, YLD-H exhibited the most optimal inhibition of splenic atopic immune responses. Data were expressed as mean ± SD (n = 10 for each group). ***$P < 0.001$.

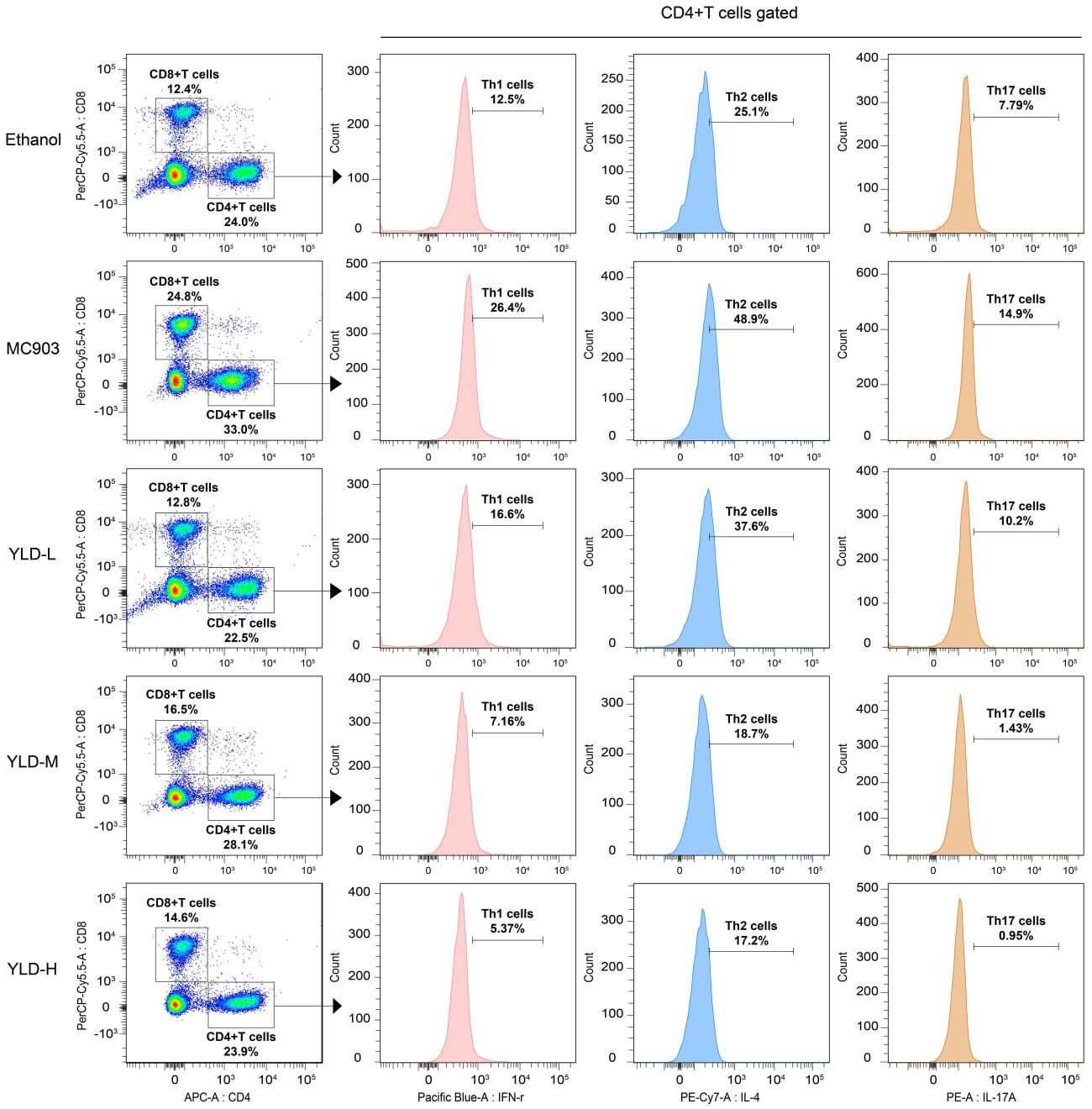

Figure 7 YLD exerted therapeutic effects in AD by modulating the balance of Th1/ Th2/ Th17 cells. YLD downregulated the CD4+/ CD8+ ratio and effectively controls the differentiation of Th1/ Th2/ Th17 cells induced by MC903 in CD4+ T cells after YLD treatment, relieving type I, type II, and type III immune responses. Furthermore, the inhibitory effect on Th cells differentiation correlated with the dose of YLD, with YLD-H exhibiting the best inhibitory effect on Th cells differentiation.

responses. Oral administration of YLD at all three dosages reduced the proportions of CD4+ T and CD8+ T cells in the spleen, indicating that YLD slowed down excessive immune responses. Moreover, YLD exerted different degrees of regulatory effects on type I, II, and III adaptive immune responses, as evidenced by the downregulation of the proportions of Th1, Th2, and Th17 cells.

Discussion

The predominant mechanisms underlying AD pathogenesis were the adaptive immune response mediated by Th cells and the downregulation of barrier genes such as LOR, FLG, and ELOVL6, leading to epidermal barrier impairment.[31] In non-

https://doi.org/10.2147/JIR.S531656

lesional phase of AD, allergen stimulation of the skin leaded to excessive scratching, initially compromising the skin barrier. This response activated epidermal langerhans cells (LCs) and dermal DCs,[32] resulting in infiltration and low-level activation of various Th cell subsets (Th1/ Th2/ Th17/ Th22).[33,34] During the acute phase of AD, Th2/ Th22 cells significantly increased and released multiple inflammatory mediators,[35] such as Th2-associated cytokines IL-4, IL-5, IL-13, IL-31, C-C motif chemokine ligand 18 (CCL18), and Th22-associated cytokines IL-22, S100A proteins, leading to acute skin inflammation.[36] The immunomodulatory cytokines IL-4 and IL-13 released by Th2 cells induce significantly reduced expression of FLG,[37] LOR,[38] and ELOVLs[39] in differentiated keratinocytes, thereby inhibiting the production of antimicrobial peptides and promoting colonization by *Staphylococcus aureus*.[40] These consequences further worsened skin barrier impairment. In the chronic phase of AD, apart from Th2/ Th22 cells, Th1/ Th17 cells contributed to epidermal remodeling and hyperplasia.[41]

The safety and efficacy of TCM in alleviating AD have been well established, and they were commonly used as an adjunctive therapy in clinical AD treatment.[42] This type of TCM formula contains plants with anti-inflammatory effects, which can exert synergistic effects through different mechanisms and then produce stable therapeutic effects.[43] This analysis revealed abundant contents of chlorogenic acid, luteoloside, and specnuezhenide in YLD. Chlorogenic acid accounted for 13.06% and specnuezhenide accounted for 8.83% of YLD, respectively. In previous studies, these components have demonstrated anti-inflammatory activity through mechanisms including inhibition of the MAPK/ERK/JNK pathway, the NF-κB pathway, and the JAK2/STAT3 pathway.[44–46] From the compositional point of view, YLD seems to have a therapeutic effect on AD. However, the pharmacological actions of YLD in the treatment of AD remain unclear and lack systematic validation.

Flow cytometry analysis showed that YLD treatment did not cause keratinocyte apoptosis, suggesting that it was not cytotoxic at commonly used doses. After specifying the concentration at which YLD had no effect on cell growth, we examined the effect of YLD on the regulation of antigen-presenting cells (APCs). T cell activation is mediated by APCs such as dendritic cells and M1-type macrophages.[47] Costimulatory molecules such as CD80 and CD86 expressed by APCs activate specific immunity by interacting with CD28 on the surface of T cells.[48,49] We confirmed in vitro that YLD inhibited the differentiation of M0-type macrophages into M1, suggesting that YLD may reduce T cell activation through this process.

In vivo study, we used the vitamin D3 analog MC903 to induce AD-like skin lesions in mice. Following the continuous application of MC903 to mice, AD-like symptoms such as ear swelling, redness, and dryness were observed. Still, these symptoms were alleviated to varying degrees by oral administration of YLD. YLD was found to reduce the thickness of the stratum corneum, and alleviated epidermal edema, thereby reducing SCORAD in mice in a dose-dependent manner, with higher doses of YLD being more effective. YLD at all doses reduced mast cell infiltration in the epidermis and dermis and attenuated MC903-induced weight loss. The above results validate the therapeutic effect of YLD on AD.

We found by western blot and immunohistochemistry that YLD reduced the elevated levels of the pro-inflammatory cytokines IL-4, IL-13, TNF-α, and TSLP, and IgE antibodies in AD-like mice, which were generally elevated in patients with moderate to severe AD. Notably, YLD may suppress pathogenic IgE production by downregulating IL-4 and IL-13, thereby inhibiting STAT6-mediated IgE class-switching in B cells.[50] Additionally, YLD promoted the expression of essential proteins involved in maintaining epidermal barrier integrity, including FLG, LOR, and ELOVL, whose expression was down-regulated in MC903-treated mouse skin. As expected, we found that YLD reduced the proportion of CD4+T cells and CD8+ T cells, and downregulated the proportion of Th1/ Th2/ Th17 cells in splenic lymphocytes. These results suggest that the mechanisms of YLD in treating AD include regulating T cell differentiation and regulating type I, II and III immune responses. The ability of YLD to inhibit the differentiation of CD4+ T cells was dose-dependent. Among the three doses of YLD, YLD-H exhibited a potent inhibitory effect on immune responses, while YLD-M had a more suitable immunomodulatory effect with the number and proportion of Th cells approaching those of normal mice. YLD-M is the equivalent dose for human clinical use, and its appropriate immunosuppressive effect meets the clinical safety requirements.

Although this work confirmed YLD efficacy in modulating Th responses and barrier repair, it remained unclear which component contributed to its anti-AD upstream signaling mechanisms. Future research will integrate existing LC-MS

phytochemical data with network pharmacology approaches to identify its critical pharmacodynamic material basis and molecular targets, and clarify the synergistic mechanisms of its multicomponent system.

Conclusions

This study demonstrated that YLD can alleviate AD skin lesions, improve the histopathological characteristics of skin tissue, downregulate the levels of pro-inflammatory cytokines in serum and tissues, upregulate the expression of barrier genes, and inhibit T cell differentiation. These findings supported the therapeutic potential of YLD in AD by maintaining skin barrier function and suppressing adaptive immune responses, while also suggesting its potential for treating other inflammatory diseases. In summary, this study provided systematic validation of the therapeutic efficacy of YLD in AD, elucidated the mechanisms underlying its action in AD treatment, and provided a basis for applying YLD in AD.

Data Sharing Statement

The datasets generated and analyzed during this study are available from the primary corresponding author, Professor Zhongjian Chen, upon reasonable request.

Ethics Approval

The animal study was carried out in strict accordance with the National Institutes of Health Guide for the Care and Use of Laboratory Animals and approved by the Ethics Committee of Shanghai Skin Disease Hospital (Tongji University, Shanghai, China) (grant number: 2021-107).

Author Contributions

All authors made a significant contribution to the work reported, whether that is in the conception, study design, execution, acquisition of data, analysis and interpretation, or in all these areas; took part in drafting, revising or critically reviewing the article; gave final approval of the version to be published; have agreed on the journal to which the article has been submitted; and agree to be accountable for all aspects of the work.

Funding

This work was supported by the National Natural Science Foundation of China [grant numbers 82305231] and the Science and Technology Commission of Shanghai Municipality [grant numbers 21S21900900 and 22S21902700].

Disclosure

The authors report no conflicts of interest in this work.

References

1. Stander S. Atopic Dermatitis. *N Engl J Med*. 2021;384(12):1136–1143. doi:10.1056/NEJMra2023911. PubMed PMID: 33761208.
2. Tokura Y, Hayano S. Subtypes of atopic dermatitis: from phenotype to endotype. *Allergol Int*. 2022;71(1):14–24. doi:10.1016/j.alit.2021.07.003. Epub 20210731. PubMed PMID: 34344611.
3. Langan SM, Irvine AD, Weidinger S. Atopic dermatitis. *Lancet*. 2020;396(10247):345–360. doi:10.1016/S0140-6736(20)31286-1. PubMed PMID: 32738956.
4. Silverberg JI, Gelfand JM, Margolis DJ, et al. Patient burden and quality of life in atopic dermatitis in US adults: a population-based cross-sectional study. *Ann Allergy Asthma Immunol*. 2018;121(3):340–347. doi:10.1016/j.anai.2018.07.006. Epub 20180716. PubMed PMID: 30025911.
5. Zhang J, Li G, Guo Q, et al. Allergens in Atopic Dermatitis. *Clin Rev Allergy Immunol*. 2025;68(1):11. doi:10.1007/s12016-025-09024-7. Epub 20250210. PubMed PMID: 39924626.
6. Gittler JK, Krueger JG, Guttman-Yassky E. Atopic dermatitis results in intrinsic barrier and immune abnormalities: implications for contact dermatitis. *J Allergy Clin Immunol*. 2013;131(2):300–313. doi:10.1016/j.jaci.2012.06.048. Epub 20250210. PubMed PMID: 22939651; PubMed Central PMCID: PMCPMC4281264.
7. Li H, Zhang Z, Zhang H, Guo Y, Yao Z. Update on the Pathogenesis and Therapy of Atopic Dermatitis. *Clin Rev Allergy Immunol*. 2021;61(3):324–338. doi:10.1007/s12016-021-08880-3. Epub 20210802. PubMed PMID: 34338977.
8. Liu AW, Gillis JE, Sumpter TL, Kaplan DH. Neuroimmune interactions in atopic and allergic contact dermatitis. *J Allergy Clin Immunol*. 2023;151(5):1169–1177. doi:10.1016/j.jaci.2023.03.013. PubMed PMID: 37149370; PubMed Central PMCID: PMCPMC10167546.

9. Furue M. Regulation of Filaggrin, Loricrin, and Involucrin by IL-4, IL-13, IL-17A, IL-22, AHR, and NRF2: pathogenic Implications in Atopic Dermatitis. *Int J Mol Sci*. 2020;21(15). doi:10.3390/ijms21155382. Epub 20200729. PubMed PMID: 32751111; PubMed Central PMCID: PMCPMC7432778
10. van den Bogaard EH, Elias PM, Goleva E, et al. Targeting Skin Barrier Function in Atopic Dermatitis. *J Allergy Clin Immunol Pract*. 2023;11(5):1335–1346. doi:10.1016/j.jaip.2023.02.005. Epub 20230219. PubMed PMID: 36805053; PubMed Central PMCID: PMCPMC11346348.
11. Wu J, Li L, Zhang T, et al. The epidermal lipid-microbiome loop and immunity: important players in atopic dermatitis. *J Adv Res*. 2025;68:359–374. doi:10.1016/j.jare.2024.03.001. Epub 20240307. PubMed PMID: 38460775; PubMed Central PMCID: PMCPMC11785582.
12. Biedermann T, Skabytska Y, Kaesler S, Volz T. Regulation of T Cell Immunity in Atopic Dermatitis by Microbes: the Yin and Yang of Cutaneous Inflammation. *Front Immunol*. 2015;6:353. doi:10.3389/fimmu.2015.00353. Epub 20150713. PubMed PMID: 26217343; PubMed Central PMCID: PMCPMC4500098.
13. Jha MK, Han Y, Liu Z, et al. Type 2 cytokines pleiotropically modulate sensory nerve architecture and neuroimmune interactions to mediate itch. *J Allergy Clin Immunol*. 2025. doi:10.1016/j.jaci.2025.05.011. Epub 20250526. PubMed PMID: 40436117.
14. Weidinger S, Beck LA, Bieber T, Kabashima K, Irvine AD. Atopic dermatitis. *Nat Rev Dis Primers*. 2018;4(1):1. doi:10.1038/s41572-018-0001-z. Epub 20180621. PubMed PMID: 29930242.
15. Dainichi T, Kitoh A, Otsuka A, et al. The epithelial immune microenvironment (EIME) in atopic dermatitis and psoriasis. *Nat Immunol*. 2018;19(12):1286–1298. doi:10.1038/s41590-018-0256-2. Epub 20181116. PubMed PMID: 30446754.
16. Pena J, Zameza PA, Pixley JN, Remitz A, Feldman SR. A Comparison of Topical Corticosteroids and Topical Calcineurin Inhibitors for the Treatment of Atopic Dermatitis. *J Allergy Clin Immunol Pract*. 2023;11(5):1347–1359. doi:10.1016/j.jaip.2023.03.022. Epub 20230329. PubMed PMID: 36997119.
17. Freitas E, Gooderham M, Torres T. New Topical Therapies in Development for Atopic Dermatitis. *Drugs*. 2022;82(8):843–853. doi:10.1007/s40265-022-01722-2. Epub 20220521. PubMed PMID: 35596877.
18. Yang X, Kambe N, Takimoto-Ito R, Kabashima K. Advances in the pathophysiology of atopic dermatitis revealed by novel therapeutics and clinical trials. *Pharmacol Ther*. 2021;224:107830. doi:10.1016/j.pharmthera.2021.107830. Epub 20210302. PubMed PMID: 33662453.
19. Chew YL, Khor MA, Xu Z, et al. Cassia alata, Coriandrum sativum, Curcuma longa and Azadirachta indica: food Ingredients as Complementary and Alternative Therapies for Atopic Dermatitis-A Comprehensive Review. *Molecules*. 2022;27(17). doi:10.3390/molecules27175475. Epub 20220826. PubMed PMID: 36080243; PubMed Central PMCID: PMCPMC9457827.
20. Dong F, Tan J, Zheng Y. Chlorogenic Acid Alleviates Allergic Inflammatory Responses Through Regulating Th1/Th2 Balance in Ovalbumin-Induced Allergic Rhinitis Mice. *Med Sci Monit*. 2020;26:e923358. doi:10.12659/MSM.923358. Epub 20200901. PubMed PMID: 32868754; PubMed Central PMCID: PMCPMC7485287.
21. Gendrisch F, Esser PR, Schempp CM, Wolfle U. Luteolin as a modulator of skin aging and inflammation. *Biofactors*. 2021;47(2):170–180. doi:10.1002/biof.1699. Epub 20201225. PubMed PMID: 33368702.
22. Monagas M, Brendler T, Brinckmann J, et al. Understanding plant to extract ratios in botanical extracts. *Front Pharmacol*. 2022;13:981978. doi:10.3389/fphar.2022.981978. Epub 20220930. PubMed PMID: 36249773; PubMed Central PMCID: PMCPMC9561911.
23. Chen S, Saeed A, Liu Q, et al. Macrophages in immunoregulation and therapeutics. *Signal Transduct Target Ther*. 2023;8(1):207. doi:10.1038/s41392-023-01452-1. Epub 20230522. PubMed PMID: 37211559; PubMed Central PMCID: PMCPMC10200802.
24. Guerriero JL. Macrophages: their Untold Story in T Cell Activation and Function. *Int Rev Cell Mol Biol*. 2019;342:73–93. doi:10.1016/bs.ircmb.2018.07.001. Epub 20180801. PubMed PMID: 30635094.
25. Gao J, Liang Y, Wang L. Shaping Polarization Of Tumor-Associated Macrophages In Cancer Immunotherapy. *Front Immunol*. 2022;13:888713. doi:10.3389/fimmu.2022.888713. Epub 20220630. PubMed PMID: 35844605; PubMed Central PMCID: PMCPMC9280632.
26. Alam MJ, Xie L, Yap YA, Robert R. A Mouse Model of MC903-Induced Atopic Dermatitis. *Curr Protoc*. 2023;3(3):e695. doi:10.1002/cpz1.695. PubMed PMID: 36913546.
27. Leyva-Castillo JM, Hener P, Jiang H, Li M. TSLP produced by keratinocytes promotes allergen sensitization through skin and thereby triggers atopic march in mice. *J Invest Dermatol*. 2013;133(1):154–163. doi:10.1038/jid.2012.239. Epub 20120726. PubMed PMID: 22832486.
28. Tanaka Y, Yokoyama Y, Kambayashi T. Skin-derived TSLP stimulates skin migratory dendritic cells to promote the expansion of regulatory T cells. *Eur J Immunol*. 2023;53(10):e2350390. doi:10.1002/eji.202350390. Epub 20230816. PubMed PMID: 37525585; PubMed Central PMCID: PMCPMC10592182.
29. Maddur MS, Sharma M, Hegde P, et al. Human B cells induce dendritic cell maturation and favour Th2 polarization by inducing OX-40 ligand. *Nat Commun*. 2014;5:4092. doi:10.1038/ncomms5092. Epub 20140609. PubMed PMID: 24910129; PubMed Central PMCID: PMCPMC4388556.
30. Hoshino Y, Kirima K, Arichika N, et al. Long-term application of MC903 in mice prolongs the characteristic symptoms of atopic dermatitis, such as inflammation, skin barrier dysfunction, and itching. *Exp Anim*. 2025;74(2):276–285. doi:10.1538/expanim.24-0088. Epub 20241226. PubMed PMID: 39721714; PubMed Central PMCID: PMCPMC12044355.
31. Wang F, Trier AM, Li F, et al. A basophil-neuronal axis promotes itch. *Cell*. 2021;184(2):422–440. doi:10.1016/j.cell.2020.12.033. Epub 20210114. PubMed PMID: 33450207; PubMed Central PMCID: PMCPMC7878015.
32. Xiao C, Zhu Z, Zhang C, et al. A population of dermal Langerin(+) dendritic cells promote the inflammation in mouse model of atopic dermatitis. *Front Immunol*. 2022;13:981819. doi:10.3389/fimmu.2022.981819. Epub 20221003. PubMed PMID: 36304463; PubMed Central PMCID: PMCPMC9592551.
33. Iwamoto K, Numm TJ, Koch S, Herrmann N, Leib N, Bieber T. Langerhans and inflammatory dendritic epidermal cells in atopic dermatitis are tolerized toward TLR2 activation. *Allergy*. 2018;73(11):2205–2213. doi:10.1111/all.13460. Epub 20181030. PubMed PMID: 29672867.
34. De Bruyn Carlier T, Badloe FMS, Ring J, Gutermuth J, Kortekaas Krohn I. Autoreactive T cells and their role in atopic dermatitis. *J Autoimmun*. 2021;120:102634. doi:10.1016/j.jaut.2021.102634. Epub 20210420. PubMed PMID: 33892348.
35. Brunner PM, Guttman-Yassky E, Leung DY. The immunology of atopic dermatitis and its reversibility with broad-spectrum and targeted therapies. *J Allergy Clin Immunol*. 2017;139(4S):S65–S76. doi:10.1016/j.jaci.2017.01.011. PubMed PMID: 28390479; PubMed Central PMCID: PMCPMC5405702.

36. Gittler JK, Shemer A, Suarez-Farinas M, et al. Progressive activation of T(H)2/T(H)22 cytokines and selective epidermal proteins characterizes acute and chronic atopic dermatitis. *J Allergy Clin Immunol*. 2012;130(6):1344–1354. doi:10.1016/j.jaci.2012.07.012. Epub 20120827. PubMed PMID: 22951056; PubMed Central PMCID: PMCPMC3991245.
37. Honzke S, Wallmeyer L, Ostrowski A, et al. Influence of Th2 Cytokines on the Cornified Envelope, Tight Junction Proteins, and ss-Defensins in Filaggrin-Deficient Skin Equivalents. *J Invest Dermatol*. 2016;136(3):631–639. doi:10.1016/j.jid.2015.11.007. Epub 20151119. PubMed PMID: 27015451.
38. Kim BE, Leung DY, Boguniewicz M, Howell MD. Loricrin and involucrin expression is down-regulated by Th2 cytokines through STAT-6. *Clin Immunol*. 2008;126(3):332–337. doi:10.1016/j.clim.2007.11.006. Epub 20071231. PubMed PMID: 18166499; PubMed Central PMCID: PMCPMC2275206.
39. Berdyshev E, Goleva E, Bronova I, et al. Lipid abnormalities in atopic skin are driven by type 2 cytokines. *JCI Insight*. 2018;3(4). doi:10.1172/jci.insight.98006. Epub 20180222. PubMed PMID: 29467325; PubMed Central PMCID: PMCPMC5916244.
40. Geoghegan JA, Irvine AD, Foster TJ. Staphylococcus aureus and Atopic Dermatitis: a Complex and Evolving Relationship. *Trends Microbiol*. 2018;26(6):484–497. doi:10.1016/j.tim.2017.11.008. Epub 20171209. PubMed PMID: 29233606.
41. Orciani M, Campanati A, Caffarini M, et al. T helper (Th)1, Th17 and Th2 imbalance in mesenchymal stem cells of adult patients with atopic dermatitis: at the origin of the problem. *Br J Dermatol*. 2017;176(6):1569–1576. doi:10.1111/bjd.15078. Epub 20170427. PubMed PMID: 27639070.
42. Cai X, Sun X, Liu L, et al. Efficacy and safety of Chinese herbal medicine for atopic dermatitis: evidence from eight high-quality randomized placebo-controlled trials. *Front Pharmacol*. 2022;13:927304. doi:10.3389/fphar.2022.927304. Epub 20220927. PubMed PMID: 36238577; PubMed Central PMCID: PMCPMC9551201.
43. Yang Y, Zhang Z, Li S, Ye X, Li X, He K. Synergy effects of herb extracts: pharmacokinetics and pharmacodynamic basis. *Fitoterapia*. 2014;92:133–147. doi:10.1016/j.fitote.2013.10.010. Epub 20131028. PubMed PMID: 24177191.
44. Wang L, Pan X, Jiang L, et al. The Biological Activity Mechanism of Chlorogenic Acid and Its Applications in Food Industry: a Review. *Front Nutr*. 2022;9:943911. doi:10.3389/fnut.2022.943911. Epub 20220629. PubMed PMID: 35845802; PubMed Central PMCID: PMCPMC9278960.
45. Caporali S, De Stefano A, Calabrese C, et al. Anti-Inflammatory and Active Biological Properties of the Plant-Derived Bioactive Compounds Luteolin and Luteolin 7-Glucoside. *Nutrients*. 2022;14(6):1155. doi:10.3390/nu14061155. Epub 20220309. PubMed PMID: 35334812; PubMed Central PMCID: PMCPMC8949538.
46. Wang QQ, Han S, Li XX, et al. Nuezhenide Exerts Anti-Inflammatory Activity through the NF-kappaB Pathway. *Curr Mol Pharmacol*. 2021;14(1):101–111. doi:10.2174/1874467213666200611141337. PubMed PMID: 32525787; PubMed Central PMCID: PMCPMC8778660.
47. Soskic B, Jeffery LE, Kennedy A, et al. CD80 on Human T Cells Is Associated With FoxP3 Expression and Supports Treg Homeostasis. *Front Immunol*. 2020;11:577655. doi:10.3389/fimmu.2020.577655. Epub 20210108. PubMed PMID: 33488578; PubMed Central PMCID: PMCPMC7820758.
48. Buchbinder E, Hodi FS. Cytotoxic T lymphocyte antigen-4 and immune checkpoint blockade. *J Clin Invest*. 2015;125(9):3377–3383. doi:10.1172/JCI80012. Epub 20150901. PubMed PMID: 26325034; PubMed Central PMCID: PMCPMC4588295.
49. Ahmed I, Ismail N. M1 and M2 Macrophages Polarization via mTORC1 Influences Innate Immunity and Outcome of Ehrlichia Infection. *J Cell Immunol*. 2020;2(3):108–115. doi:10.33696/immunology.2.029. PubMed PMID: 32719831; PubMed Central PMCID: PMCPMC7384756.
50. Geha RS, Jabara HH, Brodeur SR. The regulation of immunoglobulin E class-switch recombination. *Nat Rev Immunol*. 2003;3(9):721–732. doi:10.1038/nri1181. PubMed PMID: 12949496.